Calcium isotope measurements using a collision cell (CC)-MC-ICP-MS

Wei Dai, Frédéric Moynier, Marine Paquet, Julien Moureau, Baptiste Debret, Julien Siebert, Yvan Gerard, Ye Zhao

Calcium isotope measurements using a collision cell (CC)-MC-ICP-MS

Wei Dai[1], Frédéric Moynier[1], Marine Paquet[1], Julien Moureau[1], Baptiste Debret[1], Julien Siebert[1], Yvan Gerard[2], Ye Zhao[2]

[1]Université de Paris, Institut de physique du globe de Paris, CNRS, 1 rue Jussieu, Paris 75005, France.
[2]Nu Instruments, Unit 74 Clywedog Road South, Wrexham Industrial Estate, Wrexham, LL13 9X, United Kingdom.

Abstract:

Calcium is a major element in terrestrial planets and has six stable isotopes, including ^{40}Ca which is a product of radioactive decay of ^{40}K ($T_{1/2}$=1.25 Gyrs). Calcium isotope geochemistry has therefore been used to trace biological and geological processes in various environments as well as radiogenic dating. However, it has been technically impossible to analyze stable and radiogenic isotopes simultaneously and high precision measurements usually require tens of micrograms of Ca. Here, we present high-precision Ca isotopic data, including the stable isotopes ^{42}Ca, ^{43}Ca and ^{44}Ca as well as the radiogenic ^{40}Ca using a Nu Sapphire multi-collector inductively-coupled-plasma mass-spectrometer (MC-ICP-MS), that is equipped with a collision cell to minimize Ar based interferences. The stable isotopic variations are reported using the delta notation ($\delta^{40/44}Ca$, $\delta^{42/44}Ca$, $\delta^{43/44}Ca$), which is the permil deviation of a given ratio from the NIST SRM 915b standard. The radiogenic excess is reported as $\varepsilon^{40}Ca$, the per ten thousand deviation of the $^{40}Ca/^{44}Ca$ ratio from the same standard, after internal normalization to the $^{42}Ca/^{44}Ca$ ratio. We tested the influence of various parameters (Ca concentration, Ca and HNO_3 concentration mismatch between sample and standard, effect of matrix elements) on the precision and accuracy of the measurements. We show that, using ~100 ng is sufficient to

obtain high precision (<100 ppm, 2SD) $\delta^{40/44}$Ca and ε^{40}Ca using a standard bracketing technique- this represents an improvement by over an order of magnitude in sensitivity compared to any previous methods. It should be noted that a limitation is that the intensities of the standard and sample must be matched very closely (better than 2%). Following this recommendation, the Ca isotopic compositions of 9 geological samples reported here is consistent with previous data. For example, the ε^{40}Ca value of GSP-2 (3.92 ± 0.48 ‰) is within error with literature data (values between 3.69 and 4.32 ‰). Using this method, it is therefore possible, for the first time, to obtain simultaneously high-precision radiogenic and stable Ca isotopes on small samples, which will certainly open up many novel applications of Ca stable isotopes.

Introduction

Calcium is the sixth most abundant element in the bulk Earth (Allègre et al., 1995) and is involved in many geological and biological processes (DePaolo, 2004; Frausto da Silva and Williams, 2001). It is the most refractory major element of the solar system with a temperature of 50 % condensation of 1517 K (Lodders, 2003) and therefore controls the accretion of the first solids (Grossman, 1972). Through its predominance in the constitution of marine carbonate sediments (e.g., calcite), it also plays a major role in controlling the carbon cycle (Amsellem et al., 2020; De La Rocha and DePaolo, 2000; Fantle and Higgins, 2014; Fantle and Tipper, 2014). Calcium has 6 stable isotopes, ^{40}Ca (96.94 w.t.%), ^{42}Ca (0.647 w.t.%), ^{43}Ca (0.135 w.t.%), ^{44}Ca (2.086 w.t.%%), ^{46}Ca (0.004 w.t.%) and ^{48}Ca (0.187 w.t.%) with ^{40}Ca being a major product of the decay of ^{40}K ($T_{1/2}$=1.25 Gyrs). Given that one of its isotopes is radiogenic (^{40}Ca), that it has many stable

isotopes spanning a large mass difference, and that its isotopes are formed by various nucleosynthetic mechanisms, there has been an early interest in Ca isotopes to study planetary formation and evolution (Russell and Papanastassiou, 1978). The measurement of Ca isotopes has been traditionally performed using thermal-ionization mass-spectrometers (TIMS), for both the study of the radiogenic and nucleosynthetic anomalies (e.g. Antonelli et al., 2019; Caro et al., 2010; He et al., 2017; Kreissig and Elliott, 2005; Lee et al., 1978; Marshall and DePaolo, 1989; Simon et al., 2009) and the stable isotopic variations by using double spike addition (Amini et al., 2009; Feng et al., 2016; Heuser et al., 2002; Huang et al., 2011; Kang et al., 2017; Lehn and Jacobson, 2015; Russell and Papanastassiou, 1978; Schmitt et al., 2013; Simon and DePaolo, 2010; Skulan and DePaolo, 1999; Wu et al., 2020). The stable isotopic data are usually reported using the δ notation against a standard that has historically been the NIST SRM 915a. However, SRM 915a is not commercially available anymore and has been replaced by the SRM 915b that is used in this study. It was previously demonstrated that the $\delta^{44/40}$Ca of the SRM 915b was 0.72 ‰ relatively to SRM 915a (Heuser and Eisenhauer, 2008), therefore, it is easy to convert the data normalized to SRM915b to SRM915a to keep the values consistent with literature.

In the present paper we will present the data as $\delta^{x/44}$Ca as:

$$\delta^{x/44}Ca = \left(\frac{\left({}^{x}Ca / {}_{44}Ca \right) sample}{\left({}^{x}Ca / {}_{44}Ca \right) SRM915b} - 1 \right) \times 1000$$

With x=40, 42, or 43. While the radiogenic input on ^{40}Ca is usually noted using the epsilon notation as:

$$\varepsilon^{40/44}Ca = \left(\frac{\left({}^{40}Ca/{}_{44}Ca\right)_{normalized}^{sample}}{\left({}^{40}Ca/{}_{44}Ca\right)_{normalized}^{SRM915b}} - 1 \right) \times 10000$$

With $({}^{40}Ca/{}^{44}Ca)_{normalized}$ representing the $^{40}Ca/^{44}Ca$ corrected from the mass-dependent isotopic fractionation after being normalized to the $^{42}Ca/^{44}Ca$ ratio using the exponential law and a $^{42}Ca/^{44}Ca$ ratio of 0.31221 (Russell and Papanastassiou, 1978).

The development of plasma mass spectrometry has allowed the precise isotopic measurement of Ca isotopes, for both stable isotope analyses (e.g. Amsellem et al., 2020; Amsellem et al., 2019; Antonelli et al., 2021; Brazier et al., 2015; Dai et al., 2020; Fantle and Higgins, 2014; Fietzke et al., 2004; Hirata et al., 2008; Li et al., 2018; Li and Han, 2021; Valdes et al., 2014) and nucleosynthetic anomalies (Schiller et al., 2018; Schiller et al., 2012). The major limitation is that the ^{40}Ca is not measurable given that ionization is achieved in an Ar plasma (for conventional MC-ICP-MS) generating an unresolvable isobaric interference on ^{40}Ca, which would require a resolution of 190,000 to resolve while a typical high-resolution that can be achieved on these instruments is less than 15,000. The approach has been to focus on the ^{42}Ca to ^{48}Ca isotopes, leaving aside 96.94 % of the Ca. The samples must be analyzed in medium or high-resolution mode to resolve some argide isobaric interferences such as $^{40}ArH^{+}_{2}$ on ^{42}Ca, hence requiring a large amount (several tens or hundreds of μg) of Ca for precise (i.e., 2SD on the $^{42}Ca/^{44}Ca$ ratio better than 100 ppm) measurements (Li et al., 2018; Schiller et al., 2012; Valdes et al., 2014). The Sapphire, a novel dual-path MC-ICP-MS equipped with a collision-cell (CC), was launched in 2017 by Nu Instruments. This collision-cell MC-ICP-MS allows the reduction of the amount of Ar^{+} and charged argides via collision and reaction with a neutral and a reactive gas.

Using the instrument located at the Institut de Physique du Globe de Paris (IPGP), France, it was recently demonstrated that high precision measurements of K isotopic compositions can be achieved using 10 times less samples than previous methods (Moynier et al., 2021). This instrument is therefore very promising for Ca isotope measurements, including the ^{40}Ca. Performing the measurements in low resolution mode allows the use of much lower amounts of samples as previously needed on both TIMS and MC-ICP-MS, and with the possibility to combine both radiogenic and stable isotope measurements. No previous work reported Ca isotopic data using a Sapphire MC-ICP-MS, although one paper reported data on Ca isotopes using a protype CC-MC-ICP-MS (Klaver et al., 2021). Klaver et al. (2021) presented very high precision data using several tens of μg of Ca (the solutions were analyzed at 5 ppm), which return a precision of ~0.03 ‰ on $\delta^{40/44}$Ca and a precision of ~0.05 ‰ on the ε^{40}Ca. However, the technical details of the method and the estimation of the errors are unpublished to date.

Here, we present the first high precision stable and radiogenic Ca isotopic data using the IPGP CC-MC-ICP-MS Nu Sapphire. We report new data obtained on 9 samples comprising international rock standards that were previously analyzed using various methods. We also report analytical tests investigating the limiting factors of the accuracy such as the effect of K (producing the isobaric KH^+ interference on ^{40}Ca), Sr (isobaric interference of $^{84}Sr^{++}$, $^{86}Sr^{++}$ and $^{88}Sr^{++}$ on ^{42}Ca, ^{43}Ca, and ^{44}Ca respectively), and other elements (Ti, La…). The mismatch of concentration between standard and samples as well as the effect of sample concentration on the precision and accuracy of the measurement were also tested.

Samples and Methods

Samples

The samples analyzed here comprise GSP-2 (granodiorite, United States Geological Survey, USGS), AGV-2 (andesite, USGS), BHVO-2 (basalt, USGS), COQ-1 (carbonatite, USGS), PCC-1 (peridotite, USGS), BIR-1 (basalt, USGS), DTS-2 (dunite, USGS), UB-N (serpentinite, Centre de Recherche Pétrographique et Géochimique, CRPG, France) and Ka10 (carbonatite, Kaisersthul, (Amsellem et al., 2020)). We also analyzed two internal Ca standards, Alpha Aesar batch 14407 lot 249290 and VWR batch 455172T and lot 219015005-01.

The selected samples cover a range of chemical and Ca isotopic compositions and all of them have been previously analyzed for their Ca isotopic compositions in multiple laboratories. Therefore, they are well suited for testing the accuracy of the Nu Sapphire measurements, as well as confirming previous results obtained on standard MC-ICPMS or TIMS.

The effect of the intensity mismatch (between 1 and 50% of mismatch) between sample and standard was tested on the SRM 915b standard. The effect of K, Sr, La and Ti has been also tested on SRM 915b by adding various amounts of each individual element. Finally, the effect of Ca concentration on the accuracy and precision of the data has been tested by analyzing Ca from 100 ppb down to 10 ppb (which for 5 replicates would represent ~500 ng to ~50 ng of Ca, respectively).

Dissolution and chemical purification

The chemical purification was conducted at the Institut de Physique du Globe de Paris (IPGP), using the method from Feng et al. (2016), in addition to which we performed an extra step to further purify Sr using an Eichrom Sr specific resin.

50 mg of whole rock powders were dissolved using concentrated HF and HCl (5:1 volume ratio) acids in 7 mL PTFE Teflon square digestion vessels with wrench top closures in an oven at 160°C for 3 days. Following evaporation of the HF and HCl, the samples were subsequently treated with a 1:1 volume mix of concentrated HCl and HNO_3 and refluxed at 140°C for 3 days in an oven. Prior study of Debret et al. (2018), comparing this method to Parr bomb dissolution techniques, has shown that it can digest all refractory phases that are present in ultramafic rocks (e.g., PCC-1 and UB-N), including spinel. Finally, samples were brought into solution in 6N HCl in closed beakers at 120°C, periodically vibrated in an ultrasonic bath, and then opened and dried at 120°C. The dried samples were redissolved in 4 mol/L HNO_3 in preparation for the chemical purification on a 250 μL of Eichrom DGA resin. After washing the columns, the samples were loaded in 1 mL of 4 mol/L HNO_3. It must be noted that the amount of rock standards loaded on the columns was evaluated to correspond to ~25 μg of Ca. The matrix elements were washed by further addition of 6.75 mL of 4 mol/L HNO_3. The Ca was collected with 3 mL of water. This procedure was performed twice. Then the samples were further purified from Sr by passing through ~100 μL of Eichrom Sr spec resin. After washing the resin, the samples were loaded in 0.5 mL of 3 mol/L HNO_3, the calcium was then collected with an additional 1.5 mL of 3 mol/L HNO_3. This collected Ca fraction was dried down at 120°C, and several drops of concentrated HNO_3 were added and evaporated to decompose potential organic matters leached during the column chemistry. The whole procedure yield is over 99%. The samples were finally redissolved in 0.5 mol/L HNO_3 for Sapphire analysis.

Calcium isotopic measurements on the Sapphire

Principle of the Sapphire has been described in Moynier et al. (2021) and remains the same here. For Ca isotopic measurements, collision cell pathway of the Nu Sapphire was utilized (low energy, 4 kV acceleration). At the plasma source, the ions are accelerated at 4 kV, and then deflected off-axis and decelerated to a few tens eV to enter the radio frequency (RF) hexapole collision/reaction cell. The RF hexapole reduces mass bias effects compared to quadrupole-based cells due to its larger mass transmission window (Moynier et al., 2021). After the collision cell, the ions are re-accelerated to 4 kV and focused back onto the mass spectrometer source slit in the same manner as for the high energy path.

The collision cell was filled with hydrogen for the reaction, and helium as a buffer gas and to contribute to the collisional thermalisation of the ions within the cell in order to maximise transmission through the hexapole ion guide. The relative amount of He and H_2 introduced in the cell was optimised to minimise the Ar^+, ArH^+, ArH_2^+ and CaH_2^+, backgrounds (see Table 1 for the parameters used here).

The samples were introduced as solution into the mass spectrometer using an Apex Omega desolvating system fitted with a 100 µL/min PFA nebulizer (MicroFlow nebuliser, Elemental Scientific, Omaha, NE, USA) and with standard Ni dry cones ("dry plasma"). Zoom optics were used to optimize focusing and peak coincidence.

Data were collected in static mode (no peak jump), with $^{40}Ca^+$ measured in a Faraday cup (L6) connected to a pre-amplifier fitted with a 10^{10} Ω resistor while ^{42}Ca (L1), ^{43}Ca (H3) and ^{44}Ca (H6) were collected using 10^{11} Ω resistors. The intensities of the mass 41 and 43.5 ($^{87}Sr^{++}$) were monitored on the faraday cup L5 and H5 using 10^{11} Ω resistors. Each analysis consisted of a 60-second zero measurement in 0.5 mol/L HNO_3, followed by one block of 30 cycles with 5 second

integrations (Table 1). A 100 second wash was performed in 0.5 mol/L HNO_3 following each standard and sample analysis and a transfer time of 60 or 90 seconds was applied. Each sample was measured between 4 and 16 times, bracketed by the SRM 915b standard. The operating parameters of the instrument are listed in Table 1.

In these conditions, the background on the mass 40 was ~700 mV. The signal on the mass 41 was approximatively 25 mV. For comparison, the total signal for 100 ppb of Ca was over 155 V. The mass bias was corrected by measuring the samples alternatively with the SRM 915b standard solution (standard-sample bracketing).

Results and discussion

The Ca isotopic data for the samples are reported in Table 2 and Table S1 with literature data used here. Data for the analytical tests are reported in Tables S2-S5. The analytical errors are reported as the 2 standard-deviation (2SD) of the replicated measurements or as 2 times the standard error (2SE) when specified.

Accuracy and precision

We tested the accuracy of the method by measuring 9 samples that were previously analyzed for their stable Ca isotopic compositions. We further tested the effect of the concentration on the precision and accuracy by varying the concentration of Ca analyzed between 10 and 100 ppb (see below). For direct comparison of the data between different methods, we renormalized the stable isotope fractionation to obtain $\delta^{44/40}Ca_{SRM915a}$ data using a difference of 0.72 ‰ between SRM 915a and SRM 915b (e.g. Heuser and Eisenhauer, 2008). The $\delta^{44/40}Ca_{SRM915a}$ values obtained on the IPGP Sapphire at 100 ppb are consistent with data

previously obtained by either TIMS or MC-ICP-MS (standard bracketing and double spike). For the comparison, we took the average literature values (see Table S1 for the dataset and Figure 1). All samples fall on the 1:1 line (Figure 1), indicating the consistency in the absolute values obtained on the Sapphire with both previous MC-ICP-MS and TIMS measurements. The typical 2 standard deviation (2SD) obtained on samples run at 100 ppb is <0.1‰. For example, the $\delta^{44/40}Ca_{SRM915a}$ value of BHVO-2, 0.72 ± 0.07 ‰ (2SD, n=7), is within error with literature values such as 0.79 ± 0.09 ‰ (He et al., 2017), 0.76 ± 0.10 (Li and Han, 2021), or 0.76 ± 0.08 ‰ (Wu et al., 2020). We also analyzed a calcium solution of a carbonatite that has been previously analyzed on the IPGP Neptune Plus (and using a chemical purification described in Amsellem et al. 2020), Ka10 from the Kaiserstuhl volcano, Germany (Amsellem et al., 2020). The $\delta^{44/40}Ca_{SRM915a}$ calculated on the Neptune Plus was 0.37 ± 0.06 ‰ (2SD, n=4) (Amsellem et al., 2020), which is within error with the value of 0.38 ± 0.09 ‰ (2SD, n=6) acquired on the Sapphire. We also measured replicates for some samples over different mass-spectrometry sessions of the same chemical purification, for example a replicate of Ka10 returns a value of 0.38 ± 0.12 ‰ (2SD, n=6), similar to the result of 0.38 ± 0.09 ‰ (2SD, n=6) from the first analysis. We can assess the mass-dependence of the measurements using the relationship between $\delta^{40/44}Ca$ and $\delta^{42/44}Ca$ (Figure 2a) and $\delta^{43/44}Ca$ and $\delta^{42/44}Ca$ (Figure 2b), in which all the samples fall on the expected 2:1 and 1:2 lines, respectively. In Figure 2a, GSP-2 falls off the 2:1 line, due to the expected presence of radiogenic ^{40}Ca (see below).

To assess the accuracy and precision of the $\varepsilon^{40}Ca$, we focused on the composition of the USGS standard GSP-2 as it exhibits a clear ^{40}Ca excess (e.g., 3.69 ± 0.16 ‰ n=25, 2SE (He et al., 2017) and 4.32 ± 0.43 ‰ (Klaver et al., 2021)). As for the stable isotope fractionation, we further

assessed the effect of Ca concentration on the precision and accuracy (see below). For sample GSP-2 analyzed at 100 ppb, we obtained ε^{40}Ca=3.92 ± 0.48 ‰, (2SE, n=6), which is consistent with literature data. Given the fairly large radiogenic ^{40}Ca component for GSP-2, the $\delta^{44/40}Ca_{SRM915a}$ calculated in the table 2, has been based on $\delta^{42/44}$Ca rather than the $\delta^{40/44}$Ca as it is done for the other samples, to represent the mass-dependent isotopic fractionation and to be more readily compared to data obtained on traditional MC-ICP-MS.

Effect of the mismatch in HNO_3 concentration between sample and standard

The influence of the HNO_3 concentration mismatch between the samples and the standard on the accuracy of the Ca isotope composition was evaluated by analyzing the NIST SRM915b at various HNO_3 concentrations (between 1 and 5 %) against a NIST SRM915b solution in 3% HNO_3 (same concentration used throughout this study). The effect of the concentration mismatch has been previously identified for K isotopes on the Sapphire (Moynier et al., 2021). The results are reported in Figure 3 and Table S2. It appears that the $\delta^{40/44}$Ca is not affected by the concentration mismatch (Figure 3a) while δ^{42}Ca and δ^{43}Ca are more significantly affected, leading to an elevation of, for example, ~0.4 ‰ in the case of 5% HNO_3. This is also reflected in the variation of the ε^{40}Ca that correlates (R^2=0.994) with the HNO_3 concentration (Figure 3b). The origin of the effect is yet to be determined, but the different behaviors among ^{40}Ca/^{44}Ca and ^{42}Ca/^{44}Ca and ^{43}Ca/^{44}Ca are likely controlled by the abundances of the isotopes. Thus, it is paramount to analyze the Ca isotopic composition in the same HNO_3 concentration. In this study we dilute the standards and the samples using the same bottle of 3% HNO_3.

Effect of Ca concentration mismatch

To test the effect of intensity mismatch on the accuracy of the Ca isotopic data, we ran tests in which the Ca concentration of the NIST SRM 915b bracketing standard was kept at 100 ppb while the concentration of another NIST SRM 915b run as a sample varied from 50% lower to 50% higher (Figure 4 and Table S3). The $\delta^{40/44}$Ca is clearly affected by the concentration mismatch, the correlation (R^2=0.84) between the two (Figure 4a) returns $\delta^{40/44}Ca \sim 0.28\times Ca_{sample}/Ca_{standard}-0.25$. Therefore, a concentration difference of 1% would create a bias of about 0.02 ‰. ε^{40}Ca is also strongly affected by the Ca concentration mismatch, the correlation (R^2=0.99) between the two (Figure 4b) returns $\varepsilon^{40}Ca\sim -12\times Ca_{sample}/Ca_{standard}+12$ ‰. Therefore, a mismatch of ~1% creates a bias on ε^{40}Ca of ~0.12 ‰.

It is thus essential to analyze the samples with an intensity match within 1% of the bracketing standard in order to obtain accurate Ca isotopic data. When this protocol is applied, we show here that the Ca isotopic data (both $\delta^{40/44}$Ca and ε^{40}Ca) are accurate and precise. As for K isotopes (Moynier et al., 2021), the effect of the intensity mismatch is most likely due to a combination of the hexapole setup and of the high background on the mass 40, ~0.75V, compared to a signal of > 155V for a 100 ppb solution. The Ca background therefore represents ~0.5 % of the total Ca signal. It is possible that different instrumental parameters, in particular the hexapole setup, may affect this effect.

Effect of Ca concentration on accuracy and precision

To evaluate the precision and accuracy of the measurements, we analyzed BHVO-2 from 10 to 100 ppb of Ca (from 50 ng to 500 ng of Ca for 5 replicates) (Table S4, Figure 5). All the samples down to 100 ppb have similar $\delta^{40/44}$Ca values and fall within error of literature data when converted to SRM 915a (Figure 5, where the data are re-normalized to $\delta^{44/40}Ca_{SRM915a}$). The

precision is kept in the same range for the samples analyzed down to 25 ppb Ca (2SD between 0.04 and 0.07 ‰ for $\delta^{40/44}$Ca n=7). However, it doubles for the samples analyzed at 10 ppb (2SD of 0.14 ‰). We therefore suggest to analyze the samples at about 100 ppb (i.e., 500 ng of Ca consumption for 5 measurements) when the samples are not limited. The amount of sample can be reduced, when necessary, with a limited loss in precision and accuracy. This represents a major improvement compared to any previous methods where several tens of micrograms were usually required to reach similar precisions.

Effect of matrix elements

We tested the effect of the presence of several elements: K, Sr, Ti, La (La is taken to represent the rare earth elements which have been suggested to affect the accuracy of Ca isotopic measurements; Sun et al. 2021) on the accuracy and precision of Ca isotopic measurements. As we are using H_2 in the collision cell, a fraction of K could combine with H_2 to produce $^{39}KH^+$ and $^{41}KH^+$ and create isobaric interferences on ^{40}Ca and ^{42}Ca, respectively. Double charged strontium isotopes $^{84}Sr^{++}$, $^{86}Sr^{++}$, and $^{88}Sr^{++}$ would create isobaric interferences on ^{42}Ca, ^{43}Ca and ^{44}Ca, respectively. We monitored and corrected for these by measuring the intensity of $^{87}Sr^{++}$ on mass 43.5.

Different amounts of K, Sr, and La were added to the SRM 915b standard solutions (100 ppb) and analyzed against an undoped SRM 915b 100 ppb solution (Table S5, Figures 6 and 7). Therefore 1 % of addition corresponds to ~1 ppb of that element in the 100 ppb Ca solution. Potassium does not seem to have any effect on the $\delta^{40/44}$Ca until it reaches 2 % (Figure 6a), which corresponds in our case to ~0.6 V of ^{41}K, above the K observed in any of the natural samples reported here. As expected by the formation of $^{39}KH^+$, the $\delta^{40/44}$Ca value increases with the

increasing K addition from 0 to 2%. However, for 5% of K addition, the $\delta^{40/44}$Ca decreases back to zero. This may reflect the combination of $^{39}KH^{+}$ interference on ^{40}Ca and a matrix effect generated by K in the plasma. Similarly, the ε^{40}Ca is not affected by K up until 2 % (Figure 6b). Unlike $\delta^{40/44}$Ca, it does not exhibit the anomaly at 5%, but instead follows a negative correlation with the amount of K (Figure 6b). In summary, a K/Ca of 1% does not affect the final Ca isotopic composition within our measurement uncertainty, while a K/Ca ratio of 2% creates a bias on $\delta^{40/44}$Ca of 0.10 ± 0.02 ‰, 2SD and a ε^{40}Ca of -0.74 ± 0.63 ‰. Therefore, we recommend to maintain K/Ca < 1% to assure precise and accurate measurements.

In the case of Sr, we report both the uncorrected and corrected values (using the $^{87}Sr^{++}$ signal measured at mass 43.5, and a fixed $^{87}Sr/^{86}Sr$ ratio of 0.71039) (Table S5). The strontium correction works well up to 0.01 % of Sr (Figure 7), corresponding to a $^{87}Sr^{++}$ signal of about 4 mV, which is 3 orders of magnitude higher than that in any of the samples reported here after chemical purification. Lanthanum and titanium have smaller matrix effects and do not create any isotopic bias up to 0.1%. However, at 1% they produce a 0.18 and 0.17 ‰ bias on $\delta^{40/44}$Ca (Table S5), respectively. Thus, it is paramount to keep the La/Ca and Ti/Ca ratios under 0.1% to obtain accurate data.

Conclusions

We presented the first Ca isotopic data reported using the Nu Sapphire dual-path collision cell-capable MC-ICP-MS connected to an Apex Omega. The Ca isotopic data (for both stable and radiogenic isotopes) are both accurate and precise. We tested the effect of various parameters including acid molarity mismatch between standard and sample, concentration mismatch, the

presence of various matrix elements including Sr and K. We also tested the accuracy and precision of the measurements at various Ca concentrations, from 10 to 100 ppb. The precision obtained at 100 ppb is comparable to previous methods but with an improvement by a factor ~10 in sensitivity (in case of 5 replicates, it corresponds to ~500 ng of Ca). We also showed that data acquired down to 10 ppb (i.e., for 5 replicates ~50 ng of Ca) are still accurate but with a loss in precision (by about a factor 2). It may however be advantageous for future works involving small amounts of materials or Ca-poor samples.

Acknowledgments:

We deeply thank the two anonymous reviewers for their constructive comments that greatly improved the quality of the work. We also thank editor Balz Kamber for his comments and efficient handling of our manuscript. F. M. thanks the DIM ACAV+ (Domaine d'Interet Majeur, Astrophysique et Condition d'Apparition de la Vie) of the region Ile de France for providing part of the funding for the Nu Sapphire. F.M. acknowledges funding from the European Research Council under the H2020 framework program/ERC Consolidator Grant Agreement (#101001282-METAL) and financial support of the UnivEarthS Labex program at Sorbonne Paris Cité (#ANR-10-LABX-0023 and #ANR-11-IDEX-0005-02). Parts of this work were supported by IPGP multidisciplinary program PARI.

References

Allègre, C.J., Poirier, J.P., Humler, E., Hofmann, A.W., 1995. The chemical composition of the Earth. Earth Planet. Sci. Lett., 134: 515-526.

Amini, M. et al., 2009. Calcium Isotopes ($\delta^{44/40}$Ca) in MPI-DING Reference Glasses, USGS Rock Powders and Various Rocks: Evidence for Ca Isotope Fractionation in Terrestrial Silicates. 33(231-247).

Amsellem, E. et al., 2020. Calcium isotopic evidence for the mantle sources of carbonatites. Science Advances, 6: 10.1126/sciadv.aba3269.

Amsellem, E., Moynier, F., Puchtel, I.S., 2019. Evolution of the Ca isotopic composition of the mantle. Geochimica et Cosmochimica Acta, 258: 195-206.

Antonelli, M., DePaolo, D.J., Chacko, T., Grew, E., Rubatto, D., 2019. Radiogenic Ca isotopes confirm post-formation K depletion of lower crust. Geochemical Perspectives Letters, 9: 43-48.

Antonelli, M. et al., 2021. Calcium isotope evidence for early Archaean carbonates and subduction of oceanic crust. Nature Communication, 12: 2534.

Brazier, J.M. et al., 2015. Calcium isotope evidence for dramatic increase of continental weathering during the Toarcian oceanic anoxic event (Early Jurassic). Earth and Planetary Science Letters, 411: 164-176.

Caro, G., Papanastassiou, D., Wasserburg, G.J., 2010. ^{40}K–^{40}Ca isotopic constraints on the oceanic calcium cycle. Earth and Planetary Science Letters, 296: 124-132.

Dai, W. et al., 2020. Calcium isotope compositions of mantle pyroxenites. Geochimica et Cosmochimica Acta, 270: 144-159.

De La Rocha, C.L., DePaolo, D.J., 2000. Isotopic evidence for variations in the marine calcium cycle over the cenozoic. Science, 289(5482): 1176-1178.

Debret, B. et al., 2018. Ore component mobility, transport and mineralization at mid-oceanic ridges: a stable isotopes (Zn, Cu and Fe) study of the Rainbow massif (Mid-Atlantic Ridge 36°14'N). Earth and Planetary Science Letters, 503: 170-180.

DePaolo, D.J., 2004. Calcium isotopic variations produced by biological, kinetic, radiogenic and nucleosynthetic processes. In: Johnson, C.M., Beard, B.L., Albarede, F. (Eds.), Geochemistry of Non-Traditional Stable Isotopes. Reviews in Mineralogy & Geochemistry, pp. 255-288.

Fantle, M.S., Higgins, J., 2014. The effects of diagenesis and dolomitization on Ca and Mg isotopes in marine platform carbonates: Implications for the geochemical cycles of Ca and Mg. Geochimica Et Cosmochimica Acta, 142: 458-481.

Fantle, M.S., Tipper, E.T., 2014. Calcium isotopes in the global biogeochemical Ca cycle: Implications for development of a Ca isotope proxy. Earth-Science Reviews, 129: 148-177.

Feng, L. et al., 2016. Calcium Isotopic Compositions of Sixteen USGS Reference Materials. Geostand. Geoanal. Res., 41: 93-106.

Fietzke, J. et al., 2004. Direct measurement of 44Ca/40Ca ratios by MC–ICP–MS using the cool plasma technique. Chemical Geology, 206: 11-20.

Frausto da Silva, J.J.R., Williams, R.J.P., 2001. The Biological Chemistry of the Elements. The Inorganic Chemistry of Life. Univ. Press, Oxford, 584 pp.

Grossman, L., 1972. Condensation in the primitive solar nebula. Geochimica et Cosmochimica Acta, 36: 597-619.

He, Y., Wang, Y., Zhu, C., Huang, S., Li, S., 2017. Mass-independent and mass-dependent Ca isotopic compositions of thirteen geological reference materials measured by thermal ionisation mass spectrometry. Geostandards and Geoanalytical Research, 41: 283-302.
Heuser, A., Eisenhauer, A., 2008. The calcium isotope composition (delta Ca-44/40) of NIST SRM 915b and NIST SRM 1486. Geostand. Geoanal. Res., 32(3): 311-315.
Heuser, A. et al., 2002. Measurement of calcium isotopes using a multicollector TIMS technique. International Journal of Mass Spectrometry, 220: 385-397.
Hirata, T. et al., 2008. Isotopic Analysis of Calcium in Blood Plasma and Bone from Mouse Samples by Multiple Collector-ICP-Mass Spectrometry. Analytical Sciences, 24(11): 1501-1507.
Huang, S., Farkas, J., Yu, G., Petaev, M.I., Jacobsen, S.B., 2011. Calcium isotopic ratios and rare earth elements abundances from refractory inclusions from the Allende CV3 chondrite. Geochimica et Cosmochimica Acta, 77: 252-265.
Kang, J.T. et al., 2017. Earth and Planetary Science Letters, 474: 128-137.
Klaver, M. et al., 2021. The Ca isotope composition of mare basalts as a probe into the heterogeneous lunar mantle. Earth and Planetary Science Letters, 570: 117079.
Kreissig, K., Elliott, T., 2005. Ca isotope fingerprints of early crust-mantle evolution. Geochim Cosmochim Acta, 69: 165-175.
Lee, T., Papanastassiou, D.A., Wasserburg, G.J., 1978. Calcium isotopic anomalies in the Allende meteorite. Astrophysical Journal, 220: L21-L25.
Lehn, G., Jacobson, A.D., 2015. Optimization of a 48Ca–43Ca double-spike MC-TIMS method for measuring Ca isotope ratios (δ44/40Ca and δ44/42Ca): limitations from filament reservoir mixing. Journal of Analytical Atomic Spectrometry 30: 1571-1581.
Li, M. et al., 2018. High-precision Ca isotopic measurement using a large geometry high resolution MC-ICP-MS with a dummy bucket. Journal of Analytical Atomic Spectrometry, 33: 707-1719.
Li, X., Han, G., 2021. One-step chromatographic purification of K, Ca, and Sr from geological samples for high precision stable and radiogenic isotope analysis by MC-ICP-MS. Journal of Analytical Atomic Spectrometry, 36: 676-684.
Liu F, Zhu, H., Li, X., Wang, G., Zhang, Z., 2017. Calcium Isotopic Fractionation and Compositions of Geochemical Reference Materials. Geostand. Geoanal. Res., 41: 675-688.
Lodders, K., 2003. Solar System abundances and condensation temperatures of the elements. Astrophysical Journal, 591: 1220-1247.
Marshall, B., DePaolo, D.J., 1989. Calcium isotopes in igneous rocks and the origin of granite. Geochim Cosmochim Acta, 53: 917-922.
Moynier, F. et al., 2021. Potassium isotopic composition of various samples using a dual-path collision-cell-capable multiple-collector inductively coupled plasma mass spectrometer. Chemical Geology, 571: 120144.
Russell, W.A., Papanastassiou, D.A., 1978. Calcium isotope fractionation in ion-exchange chromatography. Anal. Chem., 50: 1151-1154.
Schiller, M., Bizzarro, M., Fernandez, V., 2018. Isotopic evolution of the protoplanetary disk and the building blocks of Earth and Moon. Nature, 555: 507-510.
Schiller, M., Paton, C., Bizzarro, M., 2012. Calcium isotope measurement by combined HR-MC-ICPMS and TIMS. Journal of Analytical Atomic Spectrometry, 27: 38-49.

Schmitt, A.D. et al., 2013. Calcium isotope fractionation during plant growth under a limited nutrient supply. Geochimica Et Cosmochimica Acta, 110: 70-83.
Simon, J.I., DePaolo, D.J., 2010. Stable calcium isotopic composition of meteorites and rocky planets. Earth and Planetary Science Letters, 289(3-4): 457-466.
Simon, J.I., DePaolo, D.J., Moynier, F., 2009. Calcium isotope composition of meteorites, Earth, and Mars. Astrophysical Journal, 702: 707-715.
Skulan, J., DePaolo, D.J., 1999. Calcium isotope fractionation between soft and mineralized tissues as a monitor of calcium use in vertebrates. Proc. Nat. Acad. Sci. , 96: 13709-13713.
Sun, J., et al. 2021. Ca isotope systematics of carbonatites: insights into carbonatite source and evolution. 10.7185/geochemlet.2107
Valdes, M., Moreira, M., Foriel, J., Moynier, F., 2014. The nature of Earth's building blocks as revealed by calcium isotopes. Earth and Planetary Science Letters, 394: 135-145.
Wu, W., Xu, Y.-G., Zhang, Z.-F., Li, X., 2020. Calcium isotopic composition of the lunar crust, mantle, and bulk silicate Moon: A preliminary study. Geochim. Cosmochim. Acta, 270: 313-324.

Figure and Table Captions:

Figure 1: $\delta^{44/40}Ca_{SRM915a}$ values from the literature (see Tables 1 and S2) plotted against the values obtained on the Nu Sapphire. The dotted line represents a 1:1 line. Data points from most samples fall on the line, which confirms that the data obtained on the Sapphire are consistent with those from the literature.

Figure 2: $\delta^{40/44}$Ca versus $\delta^{42/44}$Ca (a) and $\delta^{43/44}$Ca versus $\delta^{42/44}$Ca (b) for the samples analyzed in this study. For $\delta^{43/44}$Ca versus $\delta^{42/44}$Ca (b), all samples fall within error on a 1:2 line, agreeing with the expected mass-dependent isotopic fractionation. For $\delta^{40/44}$Ca versus $\delta^{42/44}$Ca (a), most samples fall on the mass-dependent isotopic fractionation 2:1 line, except GSP-2, which plots off the line as it contains a clear ^{40}Ca radiogenic excess.

Figure 3: Susceptibility of the $\delta^{40/44}$Ca (a) and ε^{40}Ca (b) values to the HNO_3 concentration mismatch between sample and standard. The "sample" is SRM 915b standard dissolved in acid at various molarity from 1% to 5% HNO_3 and the bracketing standard is SRM 915b at 3% HNO_3 (molarity used in the rest of the study). Although the precision and accuracy of the $\delta^{40/44}$Ca values are not affected by the acid concentration mismatch, there is a clear effect on the accuracy of the ε^{40}Ca which correlates (R^2=0.99) with the molarity mismatch.

Figure 4: Effect of the intensity mismatch on the accuracy of the $\delta^{40/44}$Ca (a) and ε^{40}Ca (b) values. The standard (SRM 915b) is kept at 100ppb while the intensity of the "sample" (SRM 915b) is analyzed at various concentrations (from +65% to – 46%). Both $\delta^{40/44}$Ca (R^2=0.84) and ε^{40}Ca (R^2=0.99) correlate with the intensity mismatch.

Figure 5: $\delta^{40/44}$Ca (a) and ε^{40}Ca (b) as a function of the Ca concentration (ppb) for BHVO-2. The stable isotopic fractionation is presented as $\delta^{44/40}Ca_{SRM915a}$ to facilitate comparison with literature data (represented by the shaded area). The accuracy of both $\delta^{44/40}Ca_{SRM915a}$ and ε^{40}Ca maintained down to 10ppb, while the precision degraded drastically for the sample analyzed at 10 ppb.

Figure 6: Effect of the K content (reported as the K/Ca in %) on the accuracy of the $\delta^{40/44}$Ca (a) and ε^{40}Ca (b) values. The x-axis represents the K content of the solution relative to the Ca concentration (100ppb for all samples) in %. The ε^{40}Ca values correlate (R^2=0.93) with the K content.

Figure 7: Effect of the Sr content (reported as Sr/Ca in %) on the accuracy of the $\delta^{40/44}$Ca (a and b) and ε^{40}Ca (c) values. The x-axis represents the Sr content of the solution relative to the Ca concentration (100 ppb for all samples) in %. In figure (a), the black circles represent the data after correcting for the Sr interference using the monitored intensity of 87^{++}. Panel (b) represents a zoom in of the Sr contents between 0 and 0.01% to illustrate that the Sr-correction is efficient in this range. Both $\delta^{40/44}$Ca (R^2=0.99) and ε^{40}Ca (R^2=0.99) correlate with the Sr content of the solution.

Table 1. Operating parameters of the Sapphire instrument and the desolvator Apex Omega introduction system.

Table 2: Calcium isotopic data of the various rock samples analyzed in this study. The literature data represent average values from: (Amini et al., 2009; Amsellem et al., 2020; Feng et al., 2016; He et al., 2017; Klaver et al., 2021; Lehn and Jacobson, 2015; Li and Han, 2021; Liu F et al., 2017; Schiller et al., 2012; Valdes et al., 2014; Wu et al., 2020).

*For GSP-2, given the radiogenic component on ^{40}Ca, $\delta^{44/40}Ca_{SRM915a}$ is calculating using the $\delta^{42/44}Ca_{value}$ rather than the $\delta^{40/44}Ca$ values has done for the other samples.

Table 1

Nu Sapphire Instrument Setting used in this study	
RF Power	1300 W
Coolant gas flow	13-13.5 L/min
Auxiliary gas flow	0.8-0.9 L/min
Sampler/skimmer cone material	Ni
He collision gas flow	2 sccm
H_2 reaction gas flow	5 sccm
Quad 1	29.1
Quad 2	-66.9
Apex parameters	
Argon Sweep Gas Flow	3.60-3.80 L/min
Nebulizer pressure	35-39.0 psi
Peripump Speed	17.0 (rpm)
Peripump Flow	600.0 (µL/min)
Nebulizer uptake rate	50 or 100 µL/min
Peltier Cooler temperature	3.0 ^{o}C
Desolvator temperature	155.0 ^{o}C
Spray chamber temperature	140 ^{o}C

Table 2

Samples	$\delta^{40/44}Ca$	2sd	$\delta^{42/44}Ca$	2sd	$\delta^{43/44}Ca$	2sd	$\varepsilon^{40}Ca$	2se	n	$\delta^{44/40}Ca_{SRM915a}$	2sd	Average literature $\delta^{44/40}Ca_{SRM915a}$	2sd
GSP-2	0.69	0.10	0.13	0.12	0.06	0.06	3.92	0.48	6	0.46*	0.10	0.53	0.49
AGV-2	-0.03	0.08	0.02	0.09	0.04	0.07	-0.79	0.32	5	0.75	0.08	0.74	0.11
BIR-1	-0.18	0.10	-0.06	0.13	-0.04	0.13	-0.51	0.44	5	0.90	0.10	0.85	0.14
DTS-2	-0.34	0.13	-0.20	0.08	-0.08	0.06	0.59	0.41	5	1.06	0.13	1.20	0.11
COQ-1	-0.03	0.07	-0.06	0.12	0.07	0.08	0.93	0.60	10	0.75	0.07	0.68	0.07
BHVO-2	0.00	0.07	0.07	0.03	0.03	0.09	-0.58	0.69	7	0.72	0.07	0.80	0.11
BHVO-2 replicate	0.00	0.08	0.01	0.08	0.02	0.19	-0.10	0.50	4	0.72	0.08		
Ka10	0.34	0.09	0.19	0.09	0.11	0.08	-1.21	0.57	6	0.38	0.09	0.37	0.03
Ka10 replicate	0.34	0.12	0.14	0.13	0.12	0.10	0.10	0.62	6	0.38	0.12	0.37	0.03
PCC-1	-0.43	0.08	-0.16	0.11	-0.09	0.13	-1.04	0.75	11	1.15	0.08	1.14	0.07
UB-N	-0.28	0.07	-0.22	0.11	-0.16	0.11	1.62	0.65	6	1.00	0.07	0.93	0.12
VWR	-0.31	0.06	-0.18	0.07	-0.09	0.06	0.60	0.89	6	1.03	0.06		
Alpha	-0.33	0.11	-0.21	0.07	-0.11	0.12	1.10	0.55	5	1.05	0.11		

Figure 1:

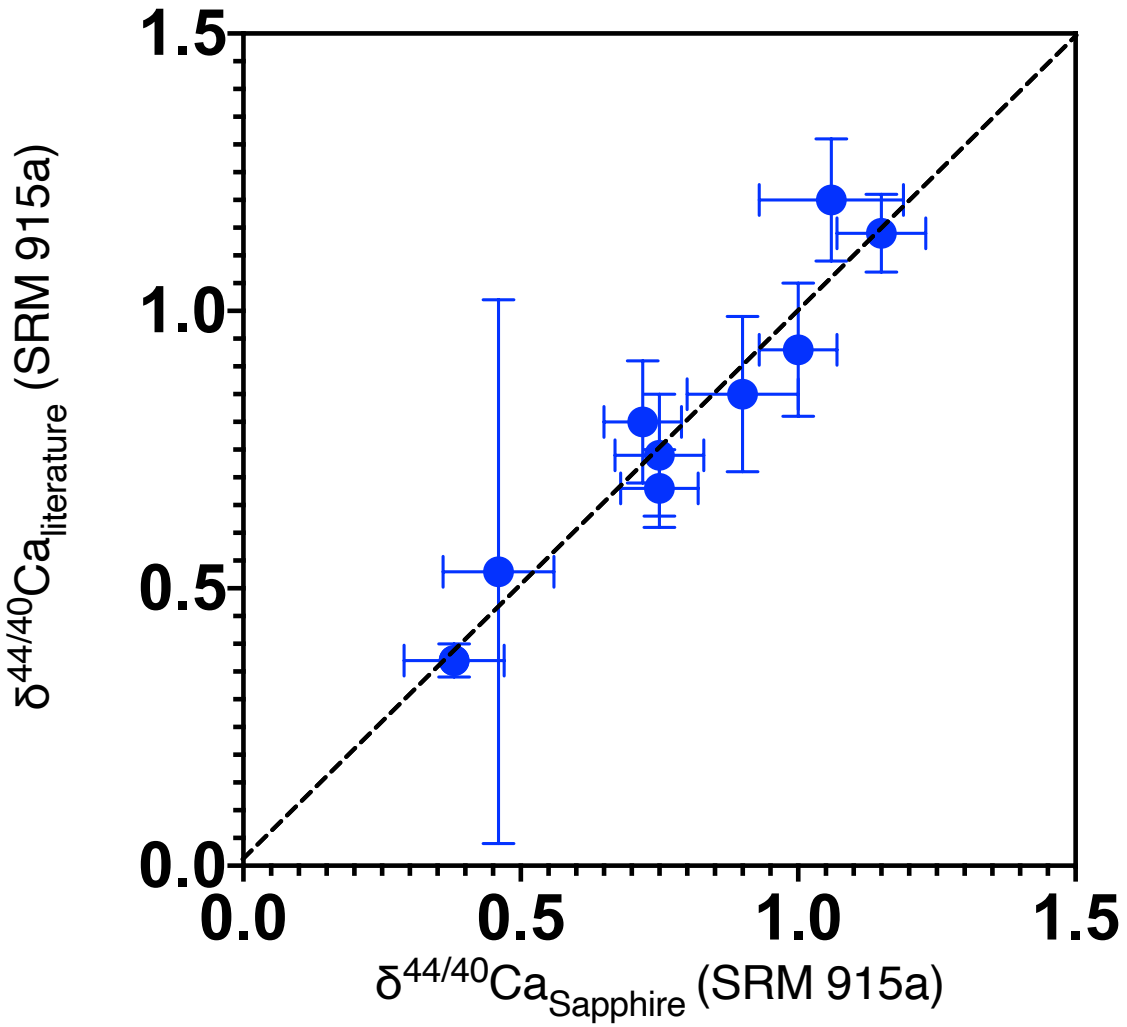

Figure 2:

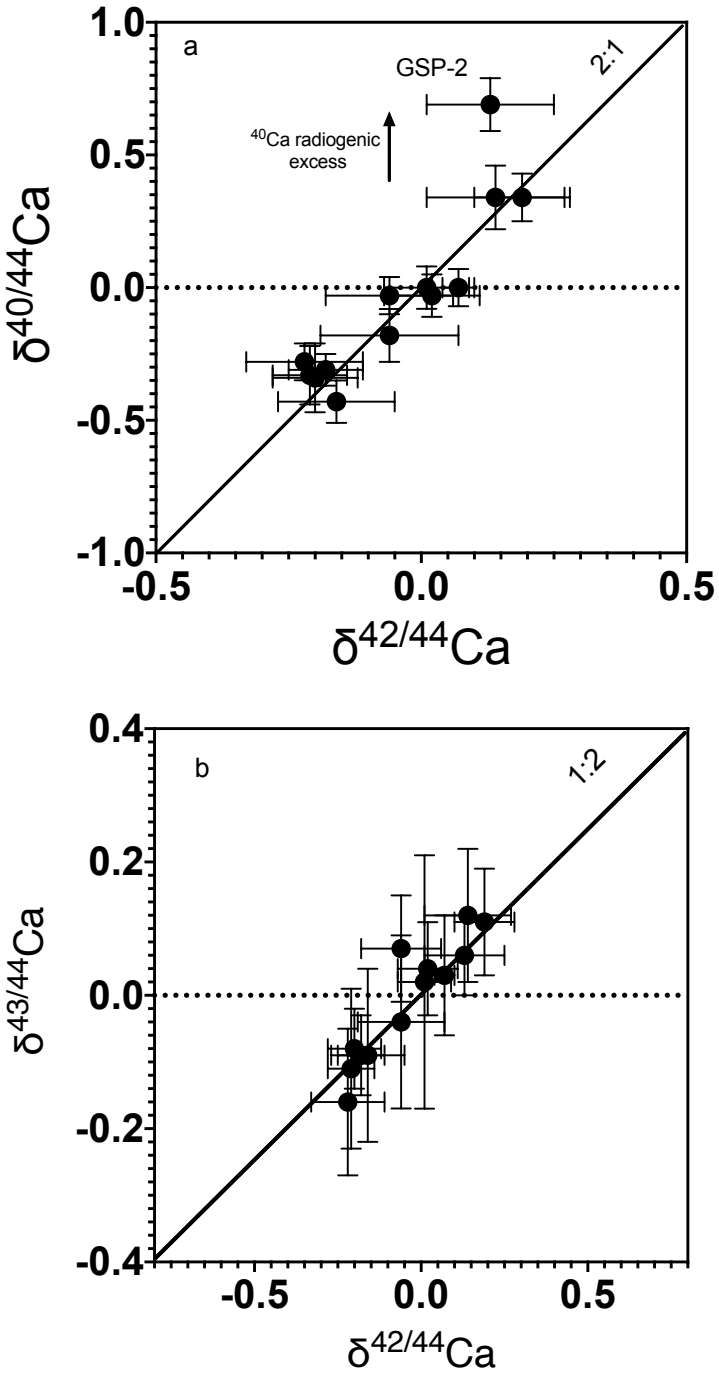

Figure 3:

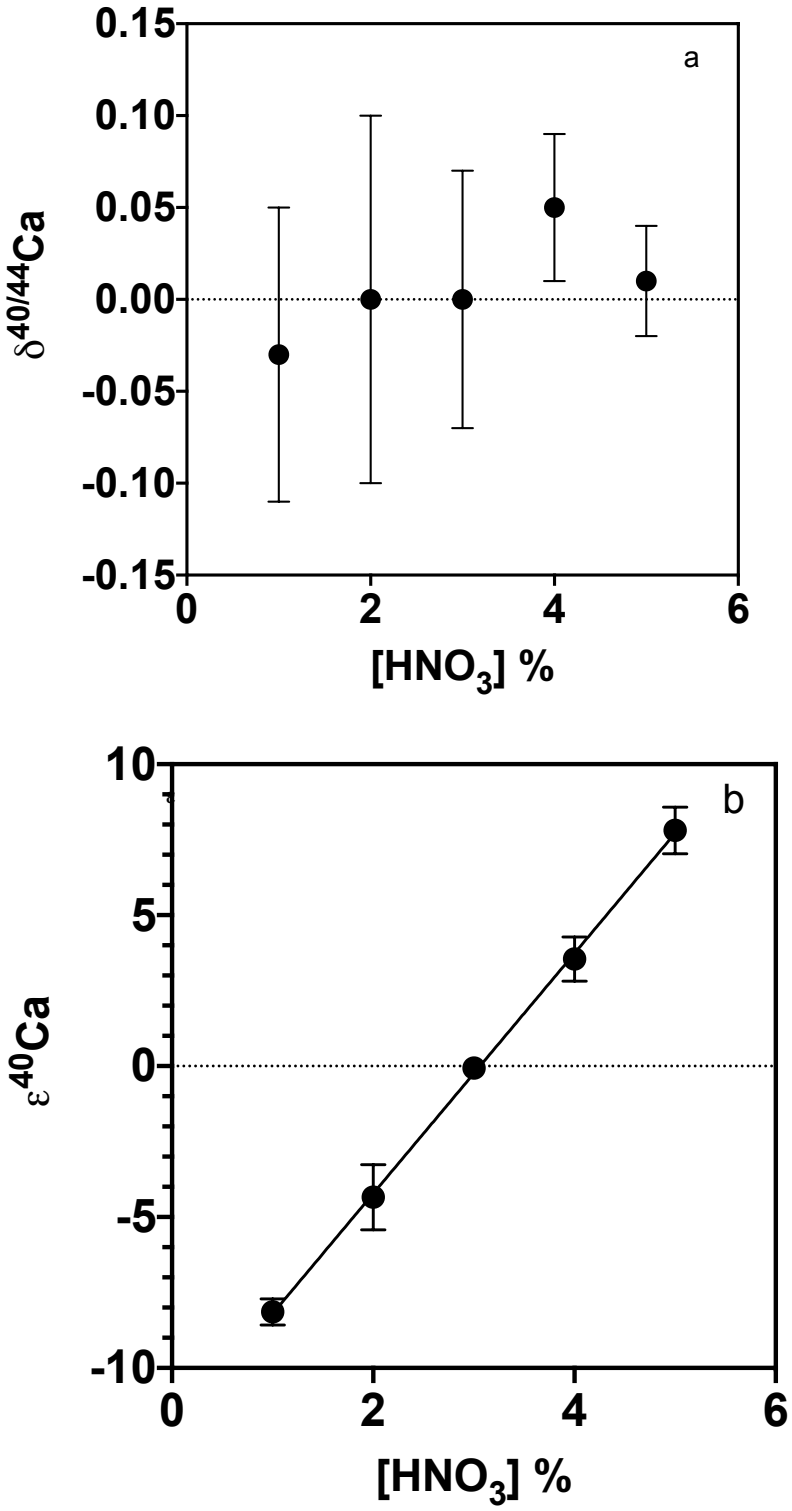

Figure 4:

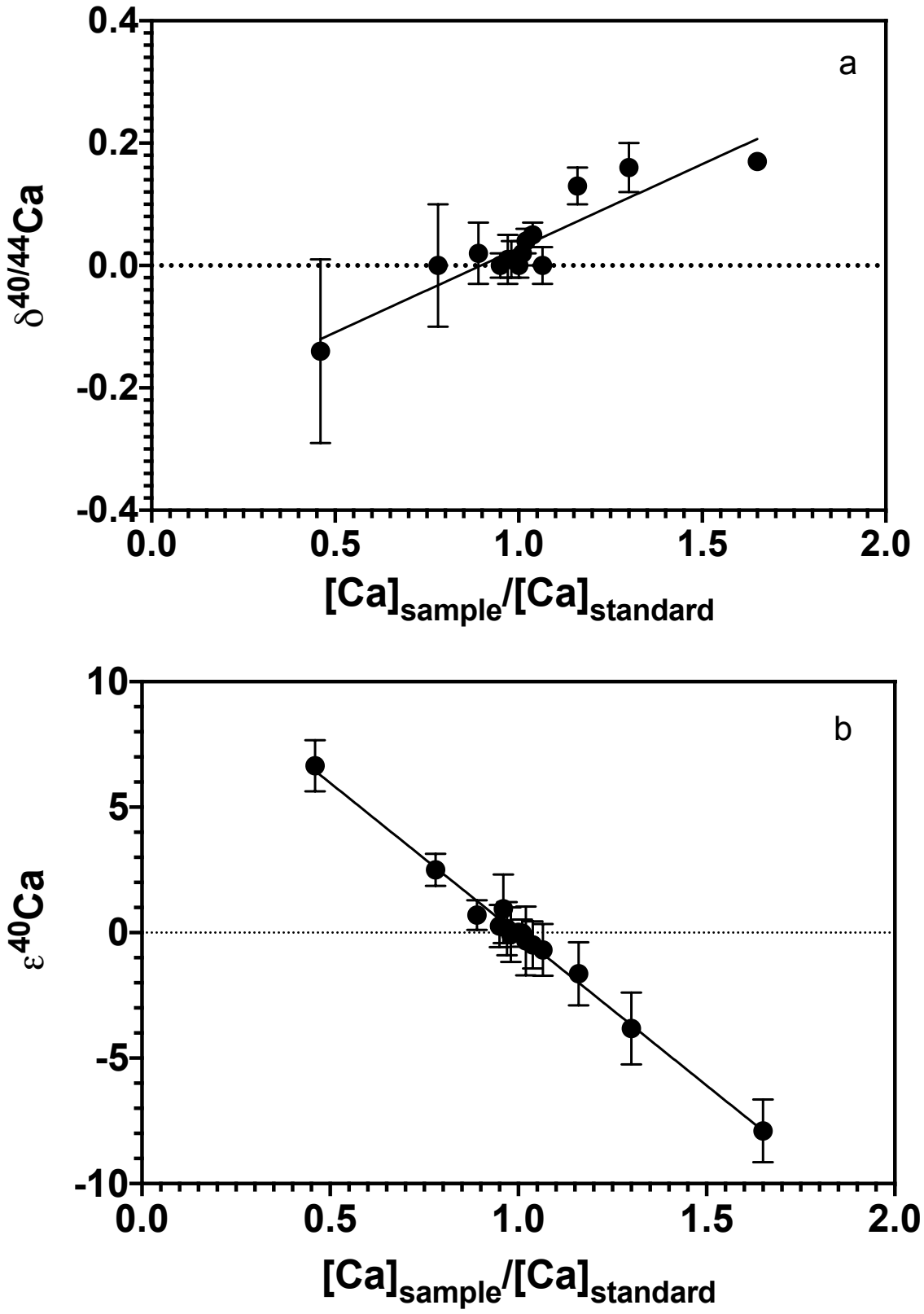

Figure 5:

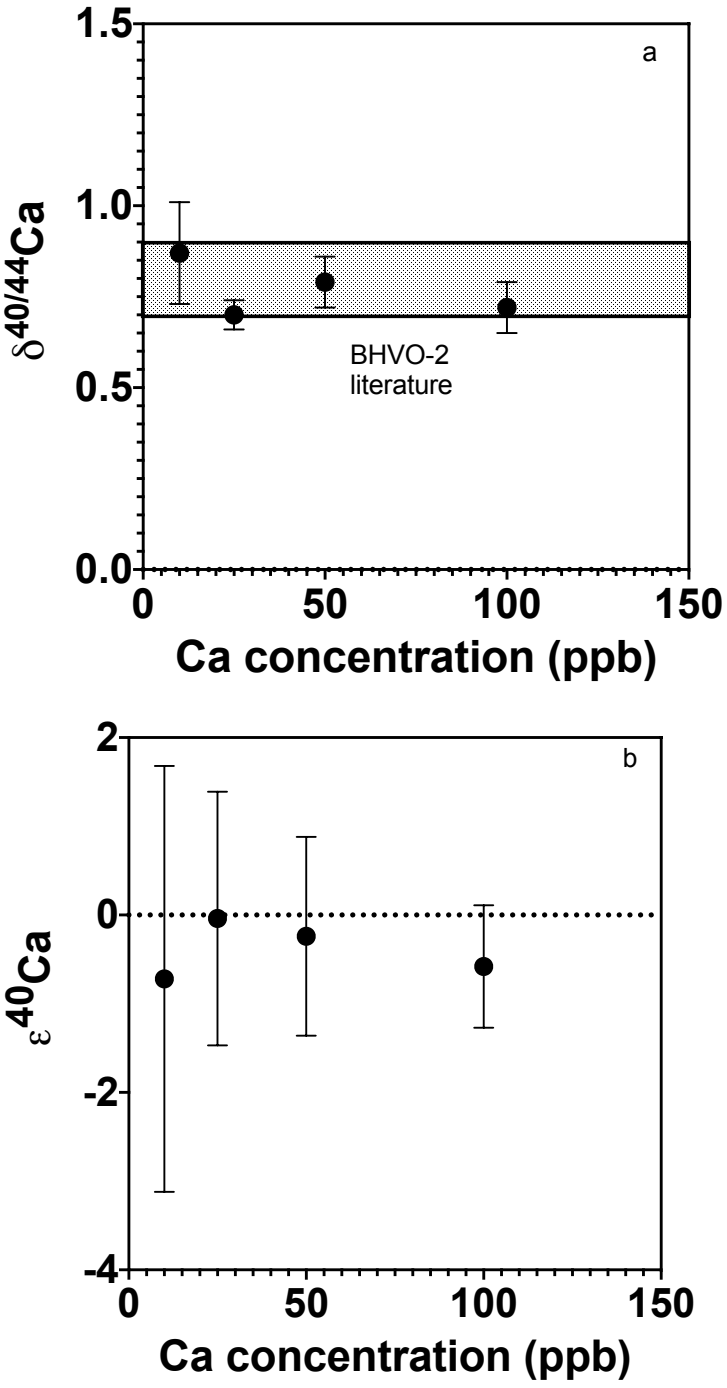

Figure 6:

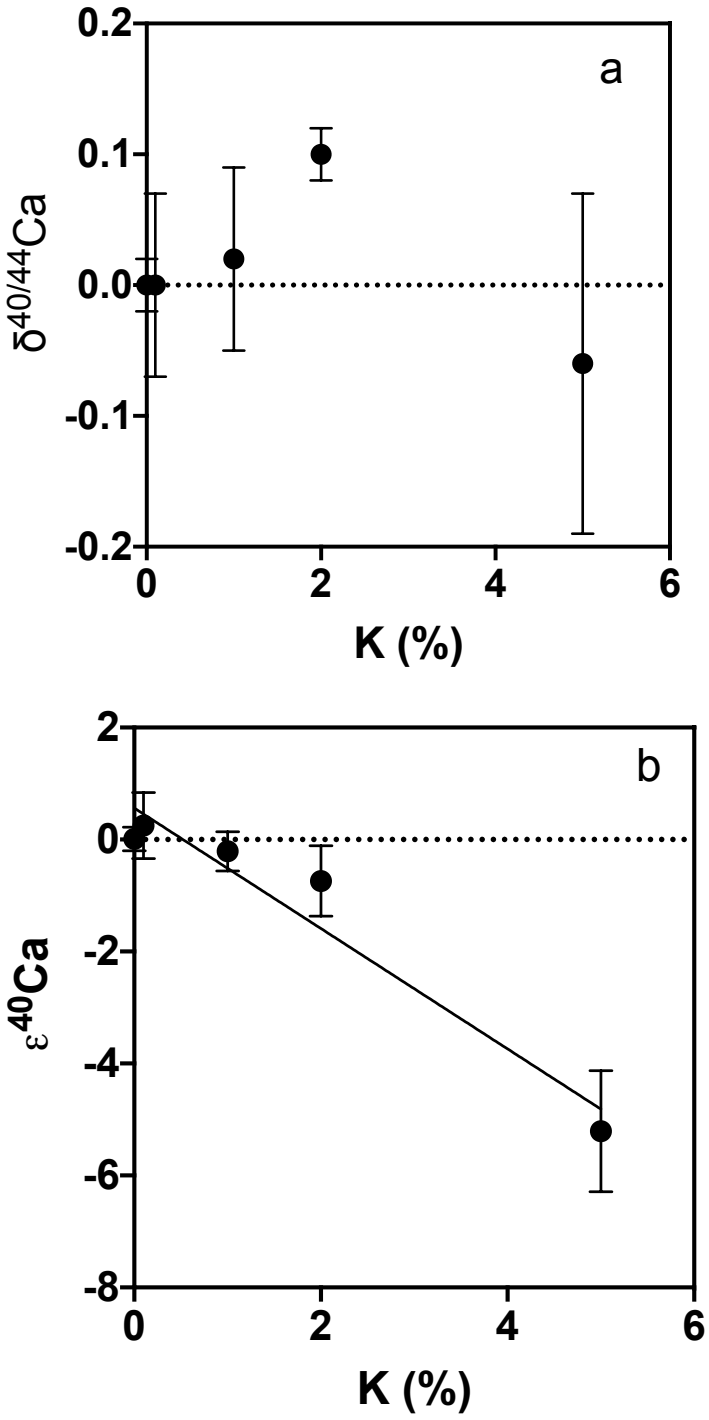

Figure 7: